J Appl Electrochem (2009) 39:1097–1103
DOI 10.1007/s10800-008-9764-3

ORIGINAL PAPER

Design of an "all solid-state" supercapacitor based on phosphoric acid doped polybenzimidazole (PBI) electrolyte

Dhanraj Rathod · Meenu Vijay · Nazrul Islam · Ramaiyan Kannan · Ulhas Kharul · Sreekumar Kurungot · Vijayamohanan Pillai

Received: 13 May 2008 / Accepted: 17 December 2008 / Published online: 8 January 2009

Abstract The effectiveness of phosphoric acid doped polybenzimidazole as a polymer electrolyte membrane to fabricate an all solid-state super capacitor has been explored using hydrous RuO_2/carbon composite electrodes (20 wt.%) of surface area 250 $m^2\ g^{-1}$ with many intrinsic advantages. The electrochemical evaluation of these super capacitors through cyclic voltammetry, charge/discharge and impedance measurements demonstrate the utility of this type of thin, compact and flexible supercapacitor capable of functioning at 150 °C to yield a maximum capacitance of about 290 F g^{-1} along with a life of more than 1,000 cycles. A power density of 300 W kg^{-1} and energy density of 10 Wh kg^{-1} have been accomplished although the equivalent series resistance (ESR) of about 3.7 Ω needs to be reduced further for high rated applications.

Keywords RuO_2/carbon composite · PBI electrolyte · Electrochemical supercapacitor · Energy storage device · Electrochemical characterization

1 Introduction

Recently, a new class of electrochemical power sources called ultracapacitors (also known as supercapacitors) has received considerable attention due to its high power density along with unique features like flexibility in charge-discharge rate modulation [1] and long cycle life [2]. These systems are useful for a variety of applications such as hybrid electric vehicles, uninterruptible power supplies, power sources for camera flash equipment, lasers and backup power sources for computer memory [3–5] due to its flexibility for varying loads. Supercapacitors are generally categorized into two classes, based on the type of electrode materials used and also the associated charge storage mechanism, as electrical double layer capacitors (EDLCs) and pseudo capacitors [6, 7]. Hybrids of electrical double layer capacitors and faradaic pseudo capacitors have also been reported as good candidates for certain applications [8–10]. The higher capacitance provided by these electrochemical capacitors (ECs) is mainly due to the enhanced surface area and adsorption features of the electroactive materials selected from many types of conducting materials such as activated carbon, carbon nanotubes, nanocomposite papers, carbon aerogels, conducting polymers and certain selected transition metal oxides [11, 12]. Among transition metal oxides, hydrous ruthenium oxide is considered as one of the best candidates for ECs, owing to its unique features, like high charge storage capacity, superior energy/ power density, excellent stability and very high conductivity [13–15]. The charge storage capacity of hydrous ruthenium oxide is through a reversible proton-electron exchange mechanism irrespective of the nature of the electrolyte as expressed by Eq. 1 [16, 17].

$$\mathrm{RuO}_x(\mathrm{OH})_y + \delta\mathrm{H}^+ + \delta e^- \leftrightarrow \mathrm{RuO}_{x-\delta}(\mathrm{OH})_{y+\delta} \quad E^\circ = 0.937\,\mathrm{V(vs.\ NHE)} \tag{1}$$

The capacitive behaviour of hydrous RuO_2 is attributable to several parameters such as surface area, water content, electronic conductivity and nanocrystalline nature [18, 19]. However, hydrous ruthenium oxide is an expensive material and hence much effort has been expended to replace ruthenium oxide by suitable cheaper nanostructured

D. Rathod · M. Vijay · N. Islam · R. Kannan · U. Kharul · S. Kurungot · V. Pillai (✉)
National Chemical Laboratory, Dr. Homi Bhabha Road, Pune 411008, India
e-mail: vk.pillai@ncl.res.in

transition metal oxides such as MnO_2, Fe_3O_4 and V_2O_5 for aqueous electrochemical supercapacitors. Recently, conducting polymers also have gained attention as potential materials for supercapacitors due to advantages like fast doping-undoping during charge-discharge, higher charge density, easy chemical/electrochemical synthesis and low cost as compared to that of noble metal oxides, carbon nanotubes, and other electrode materials. Similarly, many new classes of promising nanostructured hybrid electrodes for supercapacitors have been developed by the unique combination of organic compounds with various inorganic materials, although their cycle life and device characteristics are yet to be evaluated completely [20].

In comparison to electrode materials, polymer electrolyte membranes for supercapacitors have not received much attention despite their extensive use with distinct advantages in various applications such as fuel cells, chlor-alkali cells, solid-state sensors and catalysis [21]. The use of such a polymer membrane in electrochemical supercapacitors, instead of liquid electrolytes, ensures significant advantages like lower internal corrosion, increased device flexibility through thinner configuration, higher charging rate, higher operating potential range and easier packaging, facilitating enhanced performance for ultracapacitor stacks [22]. Hence, the replacement of liquid electrolyte (aqueous as well as organic) by a polymer electrolyte has become one of the emerging themes especially since hybrid electric vehicle applications critically depend on the performance of high rate supercapacitor banks. Consequently, many such polymer/gel composite electrolytes have been recently investigated for supercapacitor applications which include phosphoric acid or perchloric acid doped silica gel containing polymers, hybrid organic-inorganic nano composites like sulphonated poly ether-ether ketone (SPEEK), sulphonated yttria stabilized zirconia and Nafion based systems. Although, Nafion based supercapacitors have been widely studied [23–26], there are many inherent limitations such as humidity dependant proton conductivity, higher cost, moderate chemical stability and limited operating temperature (less than 80 °C). To overcome these problems, design of alternate polymer electrolytes with better mechanical, chemical and thermal stability at elevated temperatures along with higher proton conductivity under non-humidifying conditions is an urgent priority. Among various types of alternative membranes, phosphoric acid doped polybenzimidazole (PBI) is an emerging candidate primarily due to its low cost and humidity independent performance, especially after the successful demonstration as polymer electrolyte in fuel cell applications [27, 28]. However, their application for supercapacitor has not been studied to date, despite these attractive features. In this work we explore the use of phosphoric acid doped PBI as a solid polymer electrolyte for supercapacitor applications using a standard electrode composition of 20% RuO_2/carbon composite. Various techniques like thermogravimetric analysis (TGA), X-ray diffraction (XRD), cyclic voltammetry (CV), galvanostatic charge/discharge and impedance measurements have been used to correlate the performance of these supercapacitors.

2 Experimental

2.1 Sample preparation

The electroactive material (20 wt% hydrous RuO_2/C) was prepared by mixing appropriate amounts of hydrous RuO_2 (Aldrich) in Vulcan XC-72 (Cabot Corporation) followed by wet grinding and subsequent ultrasonication in isopropyl alcohol for 1 h. This was then mechanically stirred for 5 h and dried in air for 2 h at 100 °C.

2.2 Polymer electrolyte membrane

PBI membrane was synthesized from diaminobenzidene (DAB) and isophthalic acid using polyphosphoric acid (PPA) as the solvent at 200 °C for 20 h as per Scheme 1 [29].

A PBI solution with an inherent viscosity of 1.2 dl g^{-1} in conc. H_2SO_4 is used to prepare the membranes through solution casting. In brief, a 3% PBI solution in *N*, *N*-dimethylacetamide (DMAc) was cast in a vacuum oven at 80–90 °C and kept for 24 h under dry conditions. The film formed was subsequently peeled off and treated with water at 60 °C for a week to completely remove residual DMAc. The film was then dried at 100 °C under vacuum for 2 days prior to H_3PO_4 doping. Doping was carried out by immersing the membranes in 88% H_3PO_4 solution for 72 h followed again by vacuum drying at 100 °C for 2 days. The amount of phosphoric acid uptake by this procedure was about 13 moles per repetitive unit. As an amorphous thermoplastic polymer; PBI has good chemical resistance,

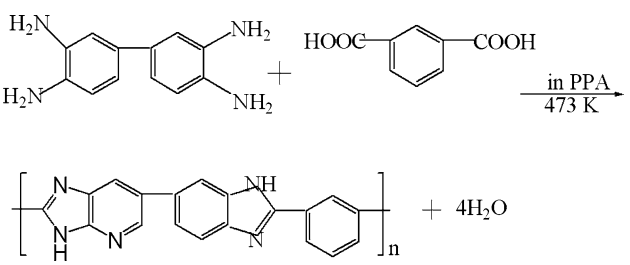

Scheme 1 Synthesis of PBI from the monomers diaminobenzidene (DAB) and Isophthalic acid using polyphosphoric acid (PPA) as the solvent

higher thermal stability (Tg ~ 437 °C) and excellent textile fiber properties.

2.3 Preparation of membrane electrode assembly

A slurry of Vulcan XC-72 (3 mg cm^{-2}) and PTFE (0.5 mg cm^{-2}) in cyclohexane, prepared by ultrasonication, was brushed on a piece of carbon cloth as a backing layer and then this electrode was cold pressed at room temperature using 0.05 tones cm^{-2} of compaction load for 3 min to make the electrode surface smooth and uniform. The carbon cloth in the electrode acts as support and an electrical current collector. Subsequently, the carbon/PTFE electrode was heat treated for 1 h at 350 °C to provide the required mechanical strength. The catalyst slurry was prepared by ultrasonicating 20% hydrous RuO_2/C composite with 1% PBI solution in DMAc. A thin layer of this slurry was applied on one side of the processed carbon cloth followed by drying. Finally, to fabricate the membrane electrode assembly (MEA) the carbon cloth was cut into two pieces of equal size (1 × 1 cm^2) and these electrodes and membranes were hot pressed uni axially at 130 °C at a compaction load of 0.05 tones cm^{-2} for 4 min to form a good ohmic contact between the electrodes and the membrane. A schematic view of this type of a single supercapacitor module fabricated using PBI electrolyte and symmetric composite electrodes along with other subcomponents is shown in Fig. 1.

3 Characterization

Thermogravimetric analysis was carried out in the range of 50–800 °C under N_2 flow at a heating rate of 5 °C min^{-1} on a Perkin-Elmer thermal analyzer to determine the thermal stability of both the electrode and electrolyte materials. A NOVA-1200 gas sorption analyzer was used to obtain the N_2 adsorption-desorption isotherm and the data were used to measure the total surface area of the composite sample by the BET method. The powder X-ray diffraction (XRD) pattern was obtained using a Rigaku Miniflex model diffractometer, equipped with a monochromatic Cu-Kα radiation ($\lambda = 0.15406$ nm, 30 kVA, 15 mA). Samples were scanned in the range 10–80° at a rate of 1° min^{-1}. Cyclic voltammetry, galvanostatic charge/discharge and impedance measurements were carried out on a single cell supercapacitor to evaluate its electrochemical performance. Cyclic voltammetry experiments were performed on a computer-controlled potentiostat (Autolab PGSTAT 30 with GPES software) using a three-electrode assembly where a Pt wire was used as the quasi-reference electrode, which was insulated through two Teflon sheets to avoid electrical shorting. RuO_2/C was employed both as the counter and working electrodes and cyclic voltammetry was carried out on this "all solid-state electrochemical system" in the potential range −0.8 to 0.7 V at different scan rates [30]. Impedance measurements were performed on a frequency response analyzer (Autolab PGSTAT 30 with FRA software) in the frequency range 100 kHz to 100 mHz with an AC signal of 10 mV amplitude. Galvanostatic charge-discharge measurements were carried out using a Solatron SI1287 electrochemical interface equipped with Corrware software. All the electrochemical measurements were performed with MEAs of PBI membrane at 150 °C.

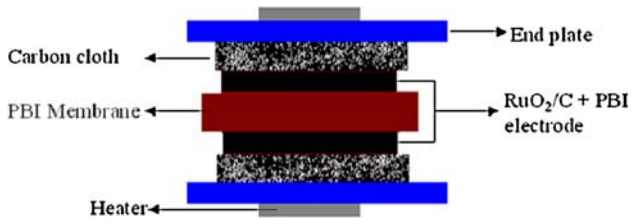

Fig. 1 Schematic representation of single cell supercapacitor with all components such as carbon cloth, electrode material, PBI membrane, and end plate with heater to reveal the stacking sequence, electrode material is made using RuO_2/carbon composite as described in the text

4 Results and discussion

4.1 Thermogravimetric analysis (TGA)

Figure 2 shows a comparison of the TGA curves obtained for both pristine and phosphoric acid doped PBI membrane electrolyte under nitrogen atmosphere. Interestingly, the phosphoric acid doped membrane shows thermal stability up to 600 °C [31]. This is in excellent agreement with the available reports on the thermal stability of PBI membranes where, the formation of strong hydrogen bonds between imidazole rings and acid molecules improves the thermal stability of the membrane after doping.

TGA curve of doped PBI membrane shows two consecutive weight loss steps; the first ~5% loss up to 200 °C is due to the loss of both free and bound water molecules in the membrane, whereas the second ~25% loss up to 750 °C is due to the dehydration of phosphoric acid.

Since the PBI membrane shows good thermal stability and the hydrous RuO_2/C mixture is used for fabricating electrodes of the MEAs made with PBI membrane, it is also important to evaluate the thermal stability of the latter for their mutual compatibility. Accordingly, Fig. 3 shows the thermal profile of RuO_2/C mixture where the first weight loss (5%) up to 273 °C is attributed to the loss of water molecules from the composite. Further degradation

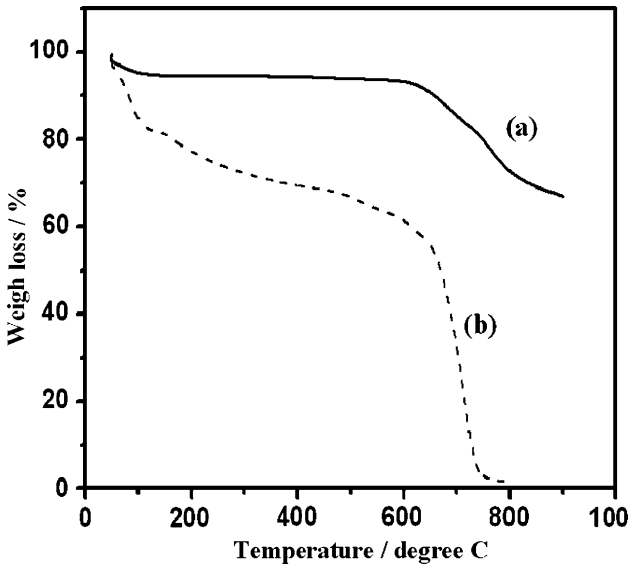

Fig. 2 Comparison of TGA curves of **a** phosphoric acid doped polybenzimidazole (PBI) membrane and **b** pristine (undoped) PBI in the range 50–800 °C. This confirms the high thermal stability of doped PBI membrane compared to that of the undoped one

of ~10% from 273 to 600 °C may be accounted for the loss of surface functional groups on the carbon support. However, complete disintegration of carbon happens at 600 °C, as can be seen from the sharp decrease in weight and, interestingly, the composite retains a residual weight of 20%, which is in accordance with the amount of RuO_2 present [32].

4.2 X-Ray diffraction (XRD)

A comparison of XRD patterns of Vulcan XC 72 carbon and a typical composite containing 20-wt. % RuO_2 is

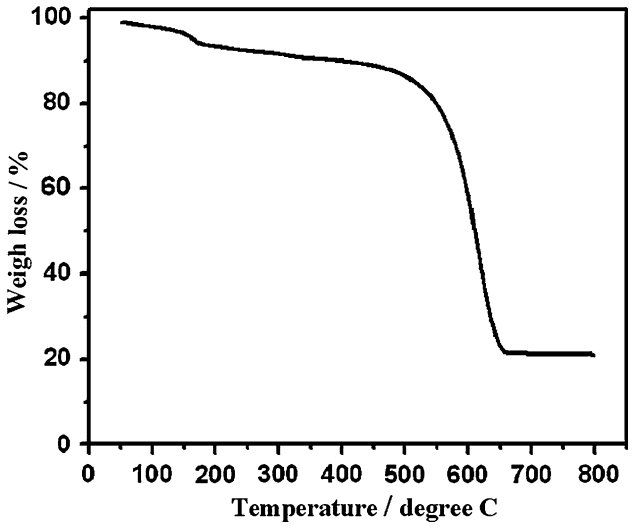

Fig. 3 TGA curve of RuO_2/carbon composite (20 wt.%RuO_2) in the range 50–800 °C which clearly shows that maximum weight loss occurs due to the desorption of water molecules

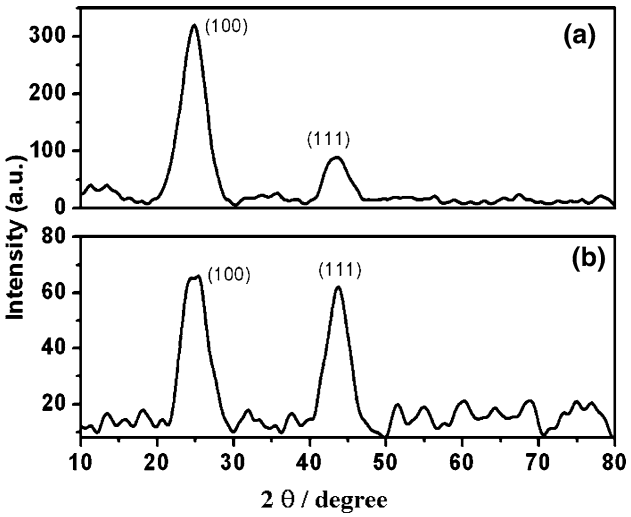

Fig. 4 Comparison of X-ray diffraction pattern for **a** Vulcan XC 72 carbon and **b** RuO_2/carbon composite in the range 10–80 °C, confirming the amorphous nature of RuO_2

presented in Fig. 4. The characteristic peaks appearing at 2θ values of 25° and 43° may be ascribed to Vulcan XC-72 carbon corresponding to (002) and (100) planes respectively, although no discernible peak is detected separately for the composite. A decrease in peak intensity of carbon with RuO_2 confirms the disordered structure of RuO_2. On the basis of such a difference in the diffraction pattern, it may be assumed that the high concentration of water in the oxide leads to a collapse of crystallinity facilitating the formation of amorphous material [32]. Hence, it may be that a part of the RuO_2 helps the electronic conduction while the structural water at the boundaries helps in proton transport [33].

These results are in excellent agreement with the data reported by Kim and Popov [34], showing that RuO_2 loaded on Vulcan XC-72 substrate displays no characteristic peaks when the composite is annealed below 150 °C. In sharp contrast, annealing RuO_2 above 200 °C generates sharp diffraction peaks due to a change in crystallinity [10]. Since PBI based supercapacitors work at 150 °C, where amorphous to crystalline phase transitions can occur in RuO_2, annealing has been carried out only at 100 °C and did not go beyond that. However, it is very important to investigate the crystallinity and structure of the composite in relation to its temperature of operation.

4.3 Cyclic voltammetry (CV)

Figure 5 shows a typical cyclic voltammogram of a PBI based supercapacitor at 5 mV s^{-1} scan rate using a platinum wire as quasi reference electrode.

A near rectangular shape suggests the good capacitative behaviour although characteristic peaks of RuO_2 do appear

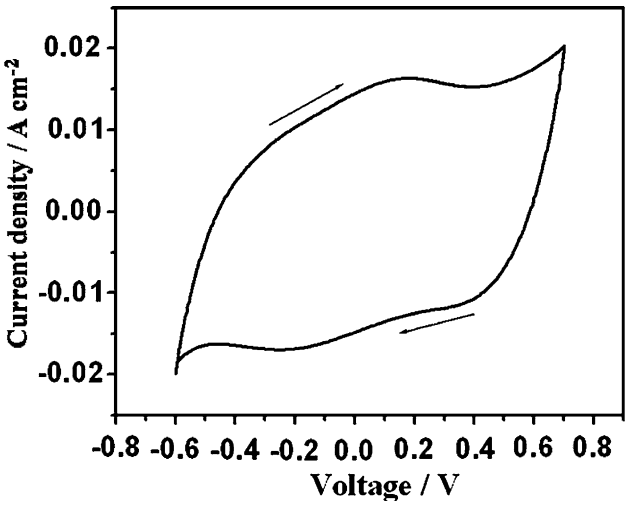

Fig. 5 Cyclic voltammogram of solid-state supercapacitor with composite electrodes taken at a scan rate of 5 mV s^{-1} illustrating the pseudo redox behaviour of RuO_2

at −0.3 and +0.1 V for reduction and oxidation, respectively. This may be attributed to the redox transition of the Ru^{+4}/Ru^{+3} couple at the electrode/PBI electrolyte interface in conjunction with Eq. 1. An approximate $E_{1/2}$ (formal potential) value of 0.2 V has been calculated for this redox couple on the basis of these broad peaks, although an unknown amount of ohmic drop might have contributed to this value.

In order to understand the variation of capacitance with scan rate, cyclic voltammograms of this supercapacitor module have been measured at different scan rates namely 5, 10, 50 and 100 mV s^{-1}. The superimposed voltammograms at these scan rates in Fig. 6 reveals that the non-faradaic current (charging current) increases with increase

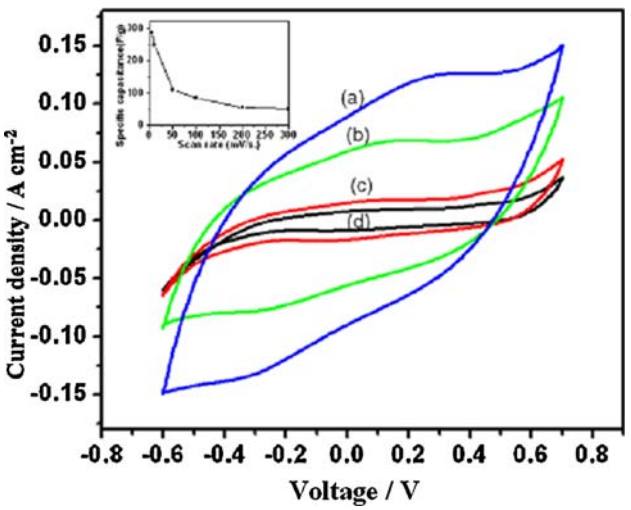

Fig. 6 Cyclic voltammograms of solid-state supercapacitor with composite electrodes and PBI electrolyte at various scan rates **a** 100, **b** 50, **c** 10, and **d** 5 mV s^{-1}; inset shows the variation of specific capacitance with scan rate

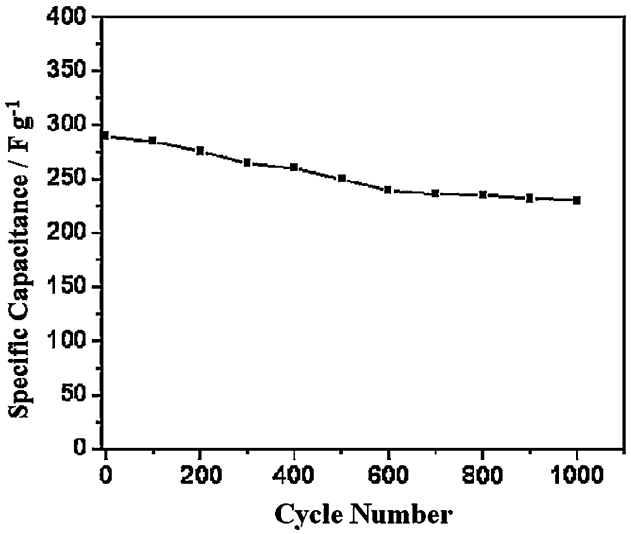

Fig. 7 Variation of the capacitance of solid-state supercapacitor fabricated with composite electrode and PBI electrolyte at 5 mV s^{-1} during 1,000 cycles

in scan rate, which clearly highlights the dependence of capacitance on scan rate (inset). However, this observed behavior could have different explanations. The first may be that the internal resistance of the device is somewhat higher, and at higher scan rate (current delivered by the capacitor is greater) a more undesirable voltage loss occurs which reduces the capacitance of the device [35, 36]. Another possible explanation is on the basis of the longer time scale required to acquire or release charge from the porous carbon electrode, leading to a higher capacitance, since the charge storage capacity increases at lower scan rates due to the influence of porosity on the RC time constant [37].

Since supercapacitors are known to have very high cycle life, it is critical to evaluate the cycling behavior of this PBI based super capacitor MEA module. Figure 7 shows the variation of specific capacitance with number of cycles evaluated for the first 1,000 cycles at 5 mV s^{-1}. Compared with an initial capacitance of 290 F g^{-1}, the capacitance after 1,000 cycles is 230 F g^{-1} (i.e., about 80% of the original capacitance) implying that an all solid-state supercapacitor with phosphoric acid doped PBI electrolyte can be operated with acceptable stability at 150 °C. This value of specific capacitance obtained from CV curves for PBI based electrolyte is superior to similar values (on the basis of weight of electroactive material for single capacitor electrode) available using other polymer electrolyte membranes [38].

4.4 Impedance techniques

Electrochemical impedance measurements were carried out in the range 100 kHz to 100 mHz in order to investigate

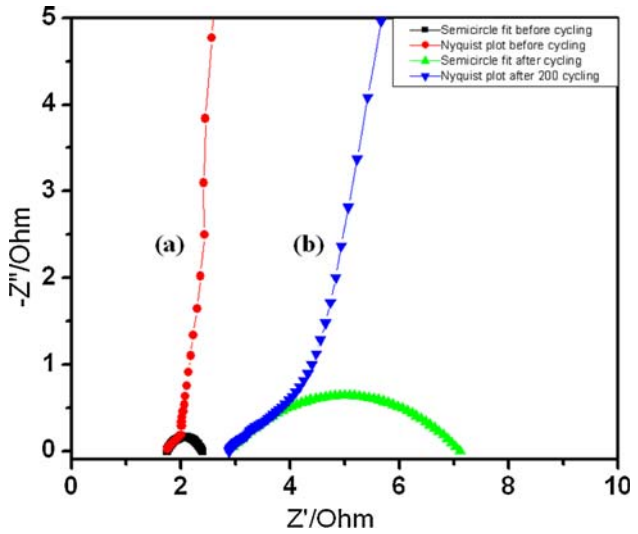

Fig. 8 Nyquist plot for solid-state supercapacitor with composite electrode and PBI electrolyte **a** before discharge **b** after discharge (200 cycles)

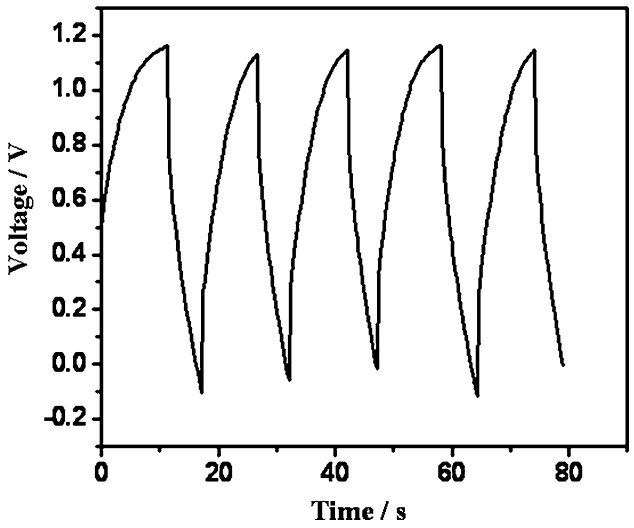

Fig. 9 Typical charge discharge curves obtained at constant current density of 2.5 mA cm^{-2} in the potential range of 0–1.2 V

the change in membrane and electrode characteristics in detail. A comparison of the impedance Nyquist plots before and after cycling is shown in Fig. 8.

By comparing Fig. 8a, b, it is clearly seen that, after cycling 1,000 times, both the electrolyte resistance and the charge transfer resistance of the supercapacitor show an interesting increase from the original values. The presence of a high frequency semicircular region with a very small radius of curvature means lower resistance to charge transfer, indicating excellent performance of this kind of a solid polymer electrolyte-electrode interface for supercapacitor applications [39]. From the point of intersecting with the real axis of the high frequency limit, the internal resistance (ESR, equivalent series resistance) of the capacitor before and after discharge was estimated as 0.85 and 1.45 $\Omega\ cm^{-1}$, respectively. The values of charge transfer resistance R_{ct} of the capacitor before and after discharge is estimated to be 0.325 and 1.0 $\Omega\ cm^{-1}$ respectively using a simple semicircle fit. However, equivalent circuit analysis using a transmission line model might be more suitable to extract better parameters in a rigorous manner.

It is obvious that, with the number of cycles, the values of both internal and charge transfer resistance of the capacitor increases leading to the deterioration in supercapacitor performance which may be attributed to a change in the properties of both electrolyte and electroactive material. These results are in excellent agreement with cyclic voltammetric results. For example, in the low frequency region, the slope of the impedance plot after discharge decreases, suggesting important changes in the mass transfer properties of the membrane after discharging.

From the equivalent series resistance (R) and the capacitance (C) of the device, it is possible to calculate the time constant (τ), which gives invaluable information on the device performance under rapid cycling conditions [32]. For instance, an RC time constant of 0.27 s calculated for this device suggests a strong need for further improvement for high rated applications.

4.5 Galvanostatic charge/discharge

Figure 9 shows a typical galvanostatic charge/discharge curve for this supercapacitor at a typical current density of ± 2.5 mA cm^{-2} in the potential range 0 to +1.2 V as a function of time. The symmetry of charge discharge characteristics shows good capacitive behavior and the ohmic drop from this is in good agreement with the value obtained from impedance measurements.

A similar response at various current densities is represented in Fig. 10, in order to indicate a direct proportionality between the current density and discharge time since higher capacitance is always obtained at a lower discharge current density. Specific energy density and power density calculated from this data are about 10 Wh kg^{-1} and 300 W kg^{-1}, respectively.

Although the performance of this type of "all solid-state" device is lower than that achieved for normal liquid electrolyte based supercapacitors, there are many advantages in terms of thinner/lighter configurations. Thus this design may have significant applications in microelectromechanical systems (MEMS). The possibility of applications at higher temperatures is also of critical importance for many Si chip based devices, despite the lower reversible voltage at higher temperatures. Nevertheless, the cycle life is insufficient for practical

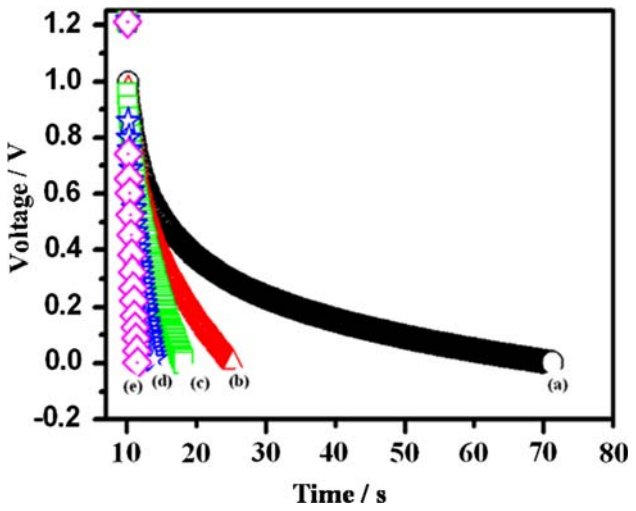

Fig. 10 Typical discharge curves from 0 to 1.2 V at various current densities: **a** 0.5, **b** 2.5, **c** 5, **d** 10 and **e** 25 mA cm^{-2}

applications and hence one of the major challenges is to develop thinner polymer membranes with higher proton conductivity.

5 Conclusions

A single cell supercapacitor device operating in the range 0–1.2 V based on hydrous RuO_2/carbon composite electrode material (220 m^2 g^{-1}) and phosphoric acid doped PBI membrane electrolyte has been successfully fabricated. This shows a capacitance of $\sim$290 F g^{-1} as demonstrated by cyclic voltammetry with no major change up to about 1,000 cycles. Electrochemical impedance analysis suggests a lower resistance for charge transfer, suggesting that this type of all solid-state supercapacitor with PBI electrolyte is promising for several applications. This is further supported by the magnitude of the energy and power density (10 Wh kg^{-1} and 300 W kg^{-1}, respectively) obtained under normal charge-discharge conditions at 150 °C.

Acknowledgements The authors are grateful to the Department of Science and Technology (TIFAC wing), New Delhi, India, for financial support. RK thanks UGC for his fellowship.

References

1. Conway BE (1999) Electrochemical supercapacitors: scientific fundamentals and technological applications, 2nd edn. Kluwer Academic Publisher, New York
2. Lee BJ, Sivakkumar SR, Ko JM, Kim JH, Seong MJ, Kim DY (2007) J Power Sources 168:546
3. Adhyapak PV, Maddanimath T, Pethkar S, Chandwadkar AJ, Negi YS, Vijayamohanan K (2002) J Power Sources 109:105
4. Shukla AK, Sampath S, Vijayamohanan K (2000) Current Sci 79:1656
5. Huggins RA (2000) Solid State Ionics 134:179
6. Lin C, Ritter JA, Popov BN (1998) Electrochem Soc 145:4097
7. Burke A (2000) J Power Sources 91:37
8. Frackowiak E, Beguin F (2001) Carbon 40:1775
9. Reddy A, Ramaprabhu S (2007) J Phys Chem C 111:7727
10. Ye JS, Cui HF, Liu X, Lim TM, Zhang WD, Sheu FS (2005) Small 1:560
11. Pushparaj VL, Shaijumon MM, Kumar A, Saravanababu M, Ci LJ, Vajtai R, Nalamasu O, Ajayan PM (2007) PNAS 104:13574
12. Sivaraman P, Rath SK, Hande VR, Thakur AP, Patri M, Samui AB (2006) Synth Metals 156:1057
13. Kim H, Popov BN (2002) J Power Sources 104:52
14. Zheng JP, Jow TR (1995) J Electrochem Soc L6:142
15. Sarangapani S, Tilak BV, Chen CP (1996) J Electrochem Soc 143:791
16. McKeown DA, Hagans LP, Carette LPL, Russell AE, Swider KE, Rolison DR (1999) J Phys Chem B 103:4825
17. Zheng JP, Cygan PJZ, Jow TR (1995) J Electrochem Soc 142:2699
18. Ramani M, Haran BS, White RE, Popov BN (2000) J Electrochem Soc 148:374
19. Ramani M, Haran BS, White RE, Popov BN, Arsov L (2000) J Power Sources 93:209
20. Murgan AV, Vijayamohanan K (2007) In: Muller A, Cheetham AK, Rao CNR (eds) Nanomaterials chemistry, 1st edn. Wiley, New York
21. Steele BCH, Heinzel A (2001) Nature 414:345
22. Lufrano F, Staiti P (2004) Electrochim Acta 49:2683
23. Osaka T, Liu X, Nojima M (1998) J Power Sources 74:22
24. Pedro GR, Chojak M, Karina CG, Asensio JA, Kulesza PJ, Nieves CP, Mónica LC (2003) Electrochem Commun 5:149
25. Sivaraman P, Hande VR, Mishra VS, Rao CS, Samui AB (2003) J Power Sources 124:351
26. Staiti P, Minutoli M, Lufrano F (2002) Electrochim Acta 47:2795
27. Kongstein OE, Berning T, Borresen B, Seland F, Tunold R (2007) Energy 32:418
28. Wainright JS, Wang JT, Weng D, Savinell RF, Litt M (1995) J Electrochem Soc 142:L121
29. Iwakura Y, Uno K, Imai Y (1964) J Poly Sci 2:2605
30. Parthasarathy M, Gopinath CS, Vijayamohanan K (2006) Chem Mater 18:5244
31. Lobato J, Canizares P, Rodrigo MA, Linares JJ, Manjavacas G (2006) J Memb Sci 280:351
32. Rolison DR, Hagans PL, Swider KE, Long JW (1998) Langmuir 15:774
33. Lyons KES, Love CT, Rolison DR (2002) J Phys Chem B 106:12677
34. Kim H, Popov BN (2001) J Power Source 104:52
35. Staiti P, Lufrano F (2005) J Electrochem Soc 152:617
36. Jang JH, Kato A, Machida K, Naoi K (2005) J Electrochem Soc 153:A321
37. Dandekar MS, Arabale G, Vijayamohanan K (2004) J Power Sources 141:198
38. Park KW, Ahn HJ, Sung YE (2002) J Power Sources 109:500
39. Wang YG, Zhang XG (2003) Solid-State Ionics 166:61